fire

MDPI

Article

Multiscale Interactions between Local Short- and Long-Term Spatio-Temporal Mechanisms and Their Impact on California Wildfire Dynamics

Stella Afolayan [1,*], Ademe Mekonnen [2,*], Brandi Gamelin [3] and Yuh-Lang Lin [2]

[1] Applied Science & Technology Ph.D. Program, North Carolina A & T State University, Greensboro, NC 27411, USA
[2] Department of Physics, North Carolina A & T State University, Greensboro, NC 27411, USA; ylin@ncat.edu
[3] Environmental Science Division, Argonne National Laboratory, Lemont, IL 60439, USA; bgamelin@anl.gov
* Correspondence: saafolayan@aggies.ncat.edu (S.A.); amekonne@ncat.edu (A.M.)

Abstract: California has experienced a surge in wildfires, prompting research into contributing factors, including weather and climate conditions. This study investigates the complex, multiscale interactions between large-scale climate patterns, such as the Boreal Summer Intraseasonal Oscillation (BSISO), El Niño Southern Oscillation (ENSO), and the Pacific Decadal Oscillation (PDO) and their influence on moisture and temperature fluctuations, and wildfire dynamics in California. The combined impacts of PDO and BSISO on intraseasonal fire weather changes; the interplay between fire weather index (FWI), relative humidity, vapor pressure deficit (VPD), and temperature in assessing wildfire risks; and geographical variations in the relationship between the FWI and climatic factors within California are examined. The study employs a multi-pronged approach, analyzing wildfire frequency and burned areas alongside climate patterns and atmospheric conditions. The findings reveal significant variability in wildfire activity across different climate conditions, with heightened risks during specific BSISO phases, La-Niña, and cool PDO. The influence of BSISO varies depending on its interaction with PDO. Temperature, relative humidity, and VPD show strong predictive significance for wildfire risks, with significant relationships between FWI and temperature in elevated regions (correlation, $r > 0.7$, $p \leq 0.05$) and FWI and relative humidity along the Sierra Nevada Mountains ($r \leq -0.7$, $p \leq 0.05$).

Keywords: wildfire; large scale; climate patterns; multiscale

Citation: Afolayan, S.; Mekonnen, A.; Gamelin, B.; Lin, Y.-L. Multiscale Interactions between Local Short- and Long-Term Spatio-Temporal Mechanisms and Their Impact on California Wildfire Dynamics. *Fire* **2024**, *7*, 247. https://doi.org/10.3390/fire7070247

Academic Editors: Shenshi Huang, Mingjun Xu and Yubo Bi

Received: 29 May 2024
Revised: 25 June 2024
Accepted: 9 July 2024
Published: 12 July 2024

1. Introduction

Wildfires have been increasing in California and the broader western US over the last two to three decades [1]. The surge in wildfire occurrences led to increased research aiming to understand contributing factors such as weather and long-term climate conditions that increase the likelihood of these events [2]. Persistent, large, synoptic-scale teleconnections leading to prolonged drought can significantly influence wildfire frequency and intensity [3–5]. In this paper, we intend to investigate the role and contributions of increased temperatures and drought conditions to California wildfires in more detail, particularly in conjunction with teleconnections.

California's wildfire regime is shaped by several factors, ranging from local weather conditions to large-scale climate patterns [6–8]. Short term extreme weather on a particular day (e.g., Santa Ana wind conditions in Southern California) to longer-term shifts in climate patterns can favor or exacerbate wildfire conditions. While local factors such as vegetation type, land use, and meteorological conditions play a crucial role, a large body of research indicates that large-scale climate fluctuations may directly or indirectly affect the likelihood of wildfires [9,10]. Keeley and Syphard [11] studied how yearly changes in burned areas in California mountains relate to seasonal weather. They found that at lower elevations

and areas with fewer forests, the yearly temperature variability did not affect the burn area. However, they showed that in forested mountains, spring and summer temperatures can influence wildfire activity [11], and that precipitation deficit increases wildfire risks, but this was not the case in California's lower elevation mountains [12]

Further studies show that the El Niño Southern Oscillation (ENSO) [13–15] is a crucial driver of climatic variability in California as it significantly influences the precipitation process, which in turn influences wildfire activity. During the La-Niña phase of ENSO, typically characterized by cooler-than-average sea surface temperatures (SSTs) in the equatorial central and eastern Pacific Ocean, California often experiences reduced rainfall, leading to drier conditions that heighten the risk of wildfires [13]. Lower precipitation during La-Niña events can lead to soil moisture deficiencies and reduced vegetation viability, increasing the risk of wildfires [16].

On the other hand, the El Niño phase, marked by warmer-than-average SSTs in the equatorial central and eastern Pacific Ocean, is often associated with increased rainfall in California [17], which can alleviate drought conditions and lower the immediate risk of wildfire by providing more moisture to soils and vegetation. However, the effects of El Niño are not uniformly beneficial; increased rainfall can lead to rapid vegetation growth, which, after drying, can provide ample fuel for wildfires in later dry months [18]. This cycle of growth and die-off can exacerbate wildfire conditions in subsequent seasons.

In addition, the interaction between ENSO and other climate phenomena, such as the Pacific Decadal Oscillation (PDO) and the Madden–Julian Oscillation (MJO), can modulate the effects of ENSO on California's climate, making the state's wildfire dynamics even more complex [14]. For example, when a negative PDO phase coincides with a strong El Niño, the warmer waters in the North Pacific can enhance the wet conditions in California, potentially reducing wildfire risks more significantly than during El Niño events alone. A notable connection is observed between unusual sea surface temperatures and sea level pressures in the central and eastern Pacific and the extent of wildfires in Florida [19]. This is shown by a strong correlation between the average SST anomaly and the variations in the burned areas, as suggested in Goddrick et al. [20]. Past work suggested a significant relationship between the prior year's ENSO conditions and the area and size of fires in subsequent years [19], suggesting the potential for an ENSO-based wildfire prediction model for California.

Apart from its interaction with ENSO, the PDO itself is a prominent large-scale climate oscillation that can potentially impact wildfire activity in California [21–23]. The PDO is a crucial climate pattern that primarily affects the mid-latitude Pacific basin. While it is often compared to the ENSO phenomenon, the PDO differs in its duration (20 to 30 years) and its significant impact on the North Pacific and North American regions. The PDO has differential effects on large-fire occurrence across different regions of the Rocky Mountains [14]. Kitzberger et al. [22] suggested that ENSO and PDO are the main influencers of wildfire variations on interannual to decadal scales, reflecting the interplay between drought, wildfires, and SST modes. However, these modes can be modulated by the alternating phases of the intraseasonal oscillation, potentially amplifying or mitigating their impacts on wildfire risk [24,25]. While the PDO and ENSO modes operate on interannual to decadal timescales, another prominent climate oscillation that may influence wildfire activity in California is the Boreal Summer Intraseasonal Oscillation (BSISO), active during the boreal summer months.

Research suggests that the BSISO, which is dominated by the MJO, plays a crucial role in driving sub-seasonal variability in the tropics throughout the boreal summer. Its convection patterns exhibit a notable northward propagation over the northern Indian Ocean and western North Pacific regions [26]. The MJO, predominantly active during the winter, exhibits a less complex spatiotemporal structure compared to the BSISO [26]. Previous studies have demonstrated that the BSISO significantly impacts the North American monsoon and influences seasonal activities in California, specifically rainfall [24,27,28].

BSISO consists of alternating phases of enhanced and suppressed convection and rainfall. The enhanced convection phase leads to stronger and more convergent wind patterns in the region [29], which lead to increased rainfall. Conversely, during the suppressed phase, high-pressure systems and anticyclonic circulation dominate, leading to weaker winds and reduced upward motion, which diminishes cloud formation and leads to drier conditions. Along with changes in wind patterns, BSISO stages also influence the transport of moisture. In the enhanced convection phase, strong winds associated with cyclonic circulation transport more moisture from the ocean to the land, contributing to increased humidity and precipitation. In contrast, during the suppressed phase, the anticyclonic circulation pattern results in reduced moisture transport from the ocean, leading to decreased humidity and lower chances of precipitation. BSISO can lead to significant shifts in the large-scale monsoon circulation [30] and, depending on its phase, can either enhance or suppress the atmospheric flow pattern, thereby affecting the transport of moisture. Prolonged dryness during the suppressed phase of the BSISO can stress plants and lower soil moisture, increasing the danger of wildfires and highlighting the importance of understanding fire weather conditions.

Fire weather is also a function of other prevailing meteorological conditions, such as wind speed and direction and lightning activity [31]. The complex interaction of these conditions with topographic features can either suppress or enhance the potential for wildfire ignition and spread [32–35]. Elevated land-based temperatures combined with low relative humidity (RH) imply drier air [2]. While humidity levels are inversely related to wildfire potential, strong wind conditions aid combustion and carry heat and embers to new areas, enabling the fire to spread rapidly [2]. High wind speeds can cause a small fire to quickly escalate into a large, uncontrollable inferno [36–39]. Understanding the dynamics of fire weather has led to the development of predictive models and indices (e.g., fire weather indices) that help authorities anticipate fire risks and allocate resources accordingly. These tools are invaluable in proactive wildfire management and resource allocation, with the fire weather index (FWI) being one of the most widely used and effective systems.

The FWI serves as an essential tool for predicting and assessing wildfire risks and is based on meteorological data [40,41]. Fire management agencies use the FWI for various operational activities, including fire prevention, preparedness planning, daily fire suppression decisions, and the allocation of firefighting resources. The FWI can help guide decisions on burning bans, fire crew staging, and aircraft deployment [42]. While the FWI system was initially developed for Canadian forests, its application has expanded globally. It has been adapted for various ecosystems, demonstrating its versatility and relevance in different climatic and vegetation conditions [43]. With the increasing impacts of climate change, the FWI is also being used in research to predict future wildfire likelihood by integrating it with climate models [44]. Observation-based studies such as this one help in understanding how wildfire danger might change in the future and allow for better preparedness. In light of the effectiveness and adaptability of the FWI system, this research intends to utilize the FWI as an important tool for a comprehensive assessment so that predicting wildfire behavior in California is possible.

In this study, we investigate the impact of large-scale and long-term climate oscillations, atmosphere–ocean anomalies, and moisture and temperature conditions on wildfire dynamics in California. We analyze the multiscale interactions and dependencies among various atmospheric–oceanic state fluctuations and their combined influence on exacerbating drought and temperature conditions, with the aim to better understand wildfire dynamics in the state of California. We also employ the BSISO and other indices in the annual and decadal ranges, focusing on the boreal summer season. Although wildfires occur in all seasons, the occurrences and intensity of CA wildfire increase during the summer period (June–August).

Additionally, we utilize vapor pressure deficit (VPD) to investigate wildfire risks. VPD is the difference between the amount of moisture in a unit of air and how much moisture that air can hold when saturated. It is a climatological parameter used to understand the

influence of temperature on atmospheric moisture demand to identify wildfire risks [45,46]. This measure is crucial in assessing the drying power of the air, as it directly influences evaporation rates. Higher VPD values indicate a greater propensity for moisture to evaporate from surfaces, potentially drawing it away from vegetation and soil [47], making the landscape drier and more susceptible to wildfires. In our study, the role of VPD becomes particularly relevant in the context of California's wildfire dynamics. Given the observed and projected increases in VPD-based drought indexes across the United States [48], it is imperative to consider its impact on drought conditions and temperature fluctuations, which in turn significantly influence wildfire risks.

In light of the complex interplay between various climatic factors and wildfire dynamics in California, this study seeks to address the following scientific questions:

1. How do large-scale climate oscillations like ENSO, PDO, and BSISO impact drought conditions and temperature fluctuations in California?
2. How do the combined effects of PDO and BSISO influence intraseasonal changes in the fire weather conditions?
3. What is the relationship between FWI, RH, VPD, and temperature in determining wildfire risks in California?
4. Does the relationship between FWI and climatic factors like temperature and moisture content vary geographically within California?

We analyzed California wildfire, weather, and climate data over a 40-year span, focusing on boreal summer. We scrutinized the patterns and severity of California wildfires during prolonged Pacific Ocean fluctuations. Following this, we computed VPD and moisture deficit (see Section 2.2) and utilized temperature and RH to establish linear relationships with the FWI across varying oscillation scales (e.g., BSISO, ENSO, and PDO).

2. Materials and Methods

2.1. Wildfire Data

Records for the state of California were retrieved from the Monitoring Trends in Burn Severity (MTBS) [49] for 1984–2021 for the entire state of California and 1991–2021 for specific regions within California, which are highlighted later in this section. This study focuses on the summer period, June-August (JJA). We extracted the start dates of individual wildfire events with 1000 burned acres and above (wildfire category "F-L"; see Table 1). We define the "Wildfire Onset Day" as the day when a particular location first triggers a class F-L wildfire classification, covering 1000 acres or more. This threshold is based on wildfire classification by the National Wildfire Coordinating Group (NWCG) [50].

Table 1. The NWCG wildfire classification is based on the size of acres covered by the wildfire.

Value	Description (Acres)
A	Greater than 0 but less than or equal to 0.25
B	0.26 to 9.9
C	10.0 to 99.9
D	100 to 299
E	300 to 999
F	1000 to 4999
G	5000 to 9999
H	10,000 to 4999
I	50,000 to 99,999
J	100,000 to 499,999
K	500,000 to 999,999
L	1,000,000+

We are interested in studying the largest and most complex wildfires, which fall under classes F to L covering 1000 acres and above.

We count the total number of wildfires each year across all locations in California and partition the count by the phase of ENSO or PDO (as described in Section 3.1). Similarly, we partition the wildfire count by region (R1, R2, and R3, as described later in Section 2.4). It is important to note that only the first day of a class F-L wildfire is recorded as the onset day, and subsequent growth of the wildfire into higher categories is not considered a new onset day.

We aim to gain insights into the behavior of large wildfires under different environmental conditions and understand the complexities involved in managing and containing them.

The choice of the MTBS data is related to a stated objective by the coalition of US federal and state agencies collaborating to create a standardized system to categorize wildfires by size and complexity.

2.1.1. Fire Danger Metrics

Fire Weather Index (FWI)

We obtained the fire weather index (FWI), a component of the Canadian Forest Fire Danger Rating System (CFFDRS), from the Copernicus Emergency Management Service (CEMS) [51]. The FWI is a unitless numerical rating of fire intensity intended to provide a standard measure of wildfire potential in a region. It gauges the wildfire potential by considering fuel moisture content and weather conditions. A higher FWI indicates a higher intensity of the fire. The FWI integrates the initial spread index (ISI) and the build-up index (BUI) (Figure 1) to assess daily wildfire intensity [52]. By quantifying the dryness of the forest floor and the potential wildfire behavior, the FWI provides vital information for anticipating when and where high-risk wildfire conditions can develop [53].

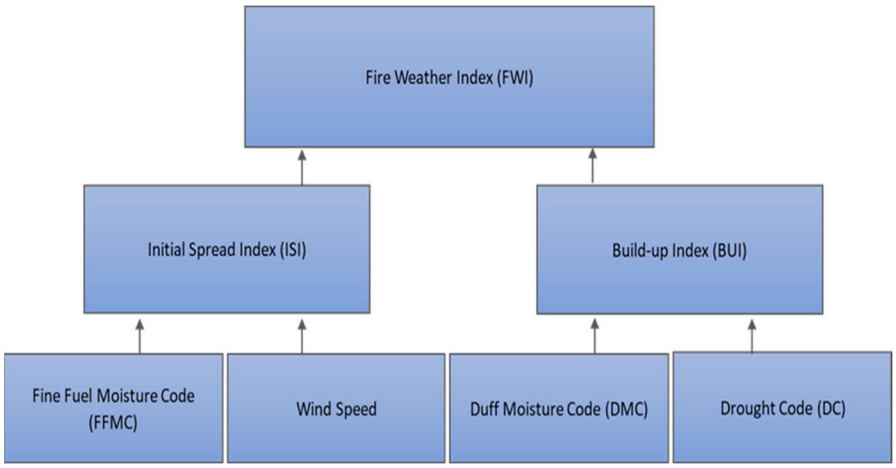

Figure 1. Flowchart illustrating how the FWI is calculated from the initial spread index and the build-up index. The ISI combines the FFMC and wind speed to calculate the estimated rate of fire spread. The ISI value usually doubles when the wind speed increases by 13 km/h [54]. The BUI, on the other hand, is a weighted combination of the DMC and DC that indicates the total amount of fuel accessible for burning by moving a flame front.

The ISI is mainly concerned with the projected rate of propagation. It considers the effects of wind and relative humidity (RH) on fine fuels in the initial phase of a wildfire. Fine fuels are small, easily ignitable materials such as leaves, grass, and twigs that can dry out quickly and are vital in determining the initial spread of a fire. It measures how rapidly a wildfire can spread after initiation. Winds enhance wildfire spread by transporting heat, flames, and embers to unburned areas. A higher ISI is often associated with a higher wind speed [54]. Fine fuels can dry out fast when exposed to wind and sun, making them more flammable. The moisture level of these small fuels is critical in influencing how quickly a wildfire spreads and is determined using the Fine Fuel Moisture Code (FFMC). A greater ISI is usually associated with a lower FFMC.

The build-up index (BUI), an integral part of the FWI, focuses on the quantity and combustibility of fuel. Composed of the Duff Moisture Code (DMC) and the Drought Code (DC) (Figure 1), it assesses the moisture levels of loosely compacted organic layers of moderate depth and deep, compact organic layers, respectively.

2.2. Weather Data

The hourly European Centre for Medium-Range Weather Forecasts (ECMWF) Reanalysis v5 (ERA5) dataset for the period 1980–2021 includes 2 m temperature, 2 m relative humidity, specific humidity, and temperature at twenty pressure levels between 1000 and 50 hPa [55]. These data, with a horizontal resolution of 0.25° × 0.25°, were averaged daily. Using the selected classes, we identified wildfire onset dates. Then, we created a composite that aligned wildfire onset days with the associated weather parameters. It is important to note that the spatial resolution of the ERA5 reanalysis dataset (0.25° × 0.25°) is much larger than the typical size of most wildfires. This discrepancy in spatial scales may introduce uncertainties in the analysis of the relationships between climate variables and wildfire occurrence, as the dataset may not capture the fine-scale variability in weather conditions that can influence wildfire behavior at the local level.

We obtained the moisture deficit (dry air) by calculating the difference between vertically integrated precipitable water and saturation precipitable water from pressure levels 1000–50 hPa. The moisture deficit measures the discrepancy between the actual atmospheric moisture content and the potential moisture the atmosphere could retain at a given temperature [56]. Precipitable water (PW) is a measure of the total mass of water vapor in a column of the atmosphere, typically expressed in kg/m^2 or millimeters (mm). It represents the depth of water that would result if all the water vapor in the column were condensed and collected at the surface. Similarly, saturated precipitable water (SPW) is a measure of the total mass of water that would be present in the column if each layer were saturated, given the same temperature profile. To calculate the moisture deficit, the atmospheric column was divided into 20 layers based on the pressure levels. For each layer, the average temperature (T), average pressure (P), and average specific humidity (q) were determined. The saturation specific humidity (qs) was calculated for each layer (Equation (2)) using the average temperature and pressure, employing the Clausius–Clapeyron equation (Equation (1)).

$$e_s = e_{s0}.exp\left(\frac{L.(T - T_0)}{R_v.T.T_0}\right) \quad (1)$$

$$q_s = \frac{0.622.e_s}{p - (1 - 0.622).e_s} \quad (2)$$

where e_s is the saturation vapor pressure in hPa, e_{s0} is the reference saturation vapor pressure at temperature T_0, L is the latent heat of vaporization, R_v is the specific gas constant for water vapor, T is the average temperature of the layer, and T_0 is the reference temperature.

The precipitable water (PW) for each layer was calculated using the following formula:

$$PW\_layer = (1/g) \times (q \times \Delta P)$$

where g is the acceleration due to gravity (9.81 m/s^2), q is the average specific humidity of the layer, and ΔP is the pressure difference across the layer. Similarly, the saturation precipitable water (SPW) for each layer was calculated using the same formula, replacing the specific humidity (q) with the saturation specific humidity (q_s). The total precipitable water (PW_total) and total saturation precipitable water (SPW_total) for the entire atmospheric column were obtained by summing the PW and SPW values for all layers, respectively. Finally, the moisture deficit was calculated by subtracting the total saturation precipitable water from the total precipitable water: Moisture Deficit = PW_total − SPW_total. The resulting moisture deficit values were expressed in millimeters (mm) and represent the

additional amount of liquid water that would need to be added to the atmospheric column to achieve saturation at the given temperature profile.

Following Gamelin et al. [48], we calculated daily vapor pressure deficit (*VPD*) using the ERA5 daily maximum temperature (T_{max}) and daily minimum relative humidity (RH_{min}) (Equations (3) and (4)).

$$e_s = 0.61080\left(17.27 * \frac{Tmax}{Tmax + 273.3}\right) \quad (3)$$

$$VPD = \left(1 - \left(\frac{RHmin}{100}\right)\right) * e_s \quad (4)$$

2.3. Atmospheric–Oceanic Indices

2.3.1. El Niño Southern Oscillation (ENSO) Index

We retrieved Multivariant ENSO Index Version 2 (MEI.V2) from the National Oceanic and Atmospheric Administration (NOAA) at https://psl.noaa.gov/enso/mei/data/meiv2.data (accessed on 13 June 2023). MEI.V2 incorporates multiple atmospheric and oceanic variables [57], such as sea surface temperatures, sea level pressures, zonal and meridional components of the surface wind, surface air temperatures, and total cloudiness fraction of the sky. We focused on the tropical Pacific region to capture the primary region of ENSO variability and its impact on the study area. We employed MEI.V2 to identify the three ENSO phases: El Niño, La-Niña, and Neutral. Using June–August (JJA) data, we categorized El Niño as index values of 0.5 or higher, La-Niña as −0.5 or lower, and Neutral for values in between, following the NOAA guidelines https://www.ncei.noaa.gov/access/monitoring/enso/sst (accessed on 13 June 2023).

2.3.2. Pacific Decadal Oscillation (PDO) Index

The PDO index is derived from monthly sea surface temperature patterns in the North Pacific Ocean, specifically from the region north of 20° N [58]. It is often described as a long-term ENSO-like pattern of Pacific climate variability and is typically calculated as the leading principal component of monthly SST anomalies in the North Pacific Ocean [58]. The PDO index was acquired from the National Centers for Environmental Information (NCEI) [58]. In our study, we considered the June–August (JJA) PDO index from 1984 to 2021. The warm (positive) PDO phase falls between 1980 and 1997, while the cool (negative) PDO phase falls from 1998 to 2021.

2.3.3. Boreal Summer Intraseasonal Oscillation (BSISO) Index

In addition, we used the BSISO index from 1980 to 2021, provided by the International Pacific Research Center (IPRC) at the University of Hawai'i at Mānoa at https://iprc.soest.hawaii.edu/users/kazuyosh/ISO_index/data/BSISO_25-90bpfil.rt_pc.txt (accessed on 15 June 2023) to monitor and measure the dominant phase of intraseasonal variability [26]. The IPRC's BSISO index is derived from comprehensive satellite observations and atmospheric reanalysis data analyses, focusing on daily anomalies in outgoing longwave radiation (OLR) and wind fields [26]. These anomalies highlight the intraseasonal oscillations in cloud cover and atmospheric circulation characteristic of the BSISO.

2.4. California Regions

California was partitioned into three distinct regions (Figure 2). Each region reflects differences, including topographic variability and climate patterns, to better investigate the differential impacts of climatic oscillations on wildfire patterns. Region 1 (R1) spans from latitudes 38° N to 42° N and longitudes 119.7° W to 124° W. This region encapsulates the northernmost part of California, characterized by a mix of coastal climates and interior valleys. The area also includes parts of the Coast Ranges, the Klamath and Northern Sierra Nevada Mountains, and the northern Central Valley, giving rise to distinctive wind patterns

influenced by the Pacific Ocean and the Bay Area's topography. These mountain ranges channel and amplify winds flowing from the Pacific Ocean, creating stronger wind patterns in the valleys and gaps. The Coastal Ranges, acting as a barrier, cause moist ocean air to rise and cool, leading to orographic precipitation on their western slopes, while creating drier conditions in rain shadow to the east [59]. Region 2 (R2) lies between latitudes 36° N to 38° N and longitudes 118° W to 122.4° W. This region predominantly covers Central California, which includes parts of the Central Valley, the Sierra Nevada Mountains, and portions of the San Francisco Bay Area. Here, the climatic patterns are influenced by both coastal and mountainous terrains, and the area experiences temperature-related wind patterns associated with valleys and the hills. Additionally, the R2 region is adjacent to the California ocean current in the eastern Pacific Ocean, which influences coastal wind and temperature patterns. Region 3 (R3) extends from latitudes 32.5° N to 36° N and longitudes 114.5° W to 121.5° W. This southernmost region encapsulates the diverse landscapes of Southern California, from the Mojave Desert to the coastal areas of Los Angeles and San Diego. The desert areas are not prone to wildfire risks. However, strong hot and dry wind systems, like the Santa Ana winds, occur along the Soledad Pass, Cajon Pass, and San Gorgonio Pass, influencing much of the R3 region. Overall, CA can be characterized by complex wind behaviors driven by its diverse geographical features.

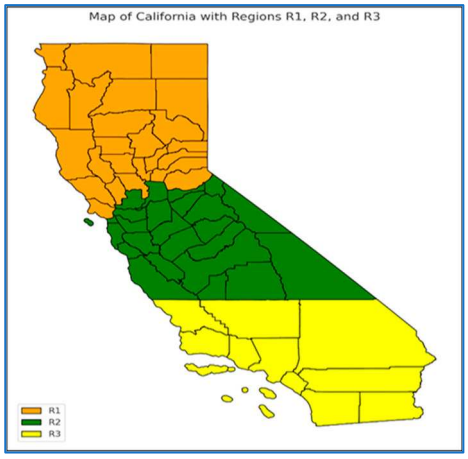

Figure 2. Map of California regions in this study: R1 (Northern California; orange), R2 (Central California; green), and R3 (Southern California; yellow).

3. Results

3.1. Frequency and Severity of CA Wildfires

Figure 3 illustrates the interannual variability in wildfire frequency and area burned in California during boreal summer (June–August). This includes wildfire events that occurred during El Niño (red), La-Niña (blue), and Neutral (black) periods, and during warm and cool PDO phases.

The top panels in Figure 3 show wildfire frequency (left) and area burned (right) under each ENSO phase. A very high number, more than 100, wildfire events were observed in 2008 during the negative phases of ENSO and PDO. The 2008 wildfire events ravaged over one million acres. Additionally, large burned areas and high frequencies occurred during the negative phases of ENSO and PDO during the 2020 and 2021 wildfire events. Of the instances where burned areas exceed the average, twice as many wildfire events occur during La-Niña compared to El Niño and Neutral: 50% during La-Niña and 25% during the El Niño and Neutral phases. This is consistent with drier and warmer conditions during the La-Niña episodic phases, as summarized in Section 1 [13].

When investigating wildfire frequency and extent across California, wildfire occurrence and area burned are not statistically significantly correlated. This, in part, suggests that not all local and large-scale factors determining wildfire initiation and containment

methods are similar. As suggested above, the highest number of wildfire incidents was reported in 2008, but with a lower frequency of occurrences, the area burned in 2020 was much higher than in 2008 (Figure 3).

Figure 3 (the lower panels) also illustrate the years corresponding to the warm and cool phases of the PDO. It is important to note that the wildfire data represented by the red bars are during a relatively brief warm PDO period (1984–1997), influenced by the constraints of available data, while those with blue bars represent a more extended cool PDO phase (1998–2021). During the 38 years, more than 50 above-average wildfire events were recorded in 14 years, predominantly during the cool PDO phase. Additionally, over time, an increase in the burned area occurred during the cool PDO phase. While areas burned before 1998 (warm PDO) are mostly below average, those after 1998 (cool PDO) are mainly above average. Above-average burn area occurs in 50% of years during the cool PDO years, compared to ~7% during the warm PDO years.

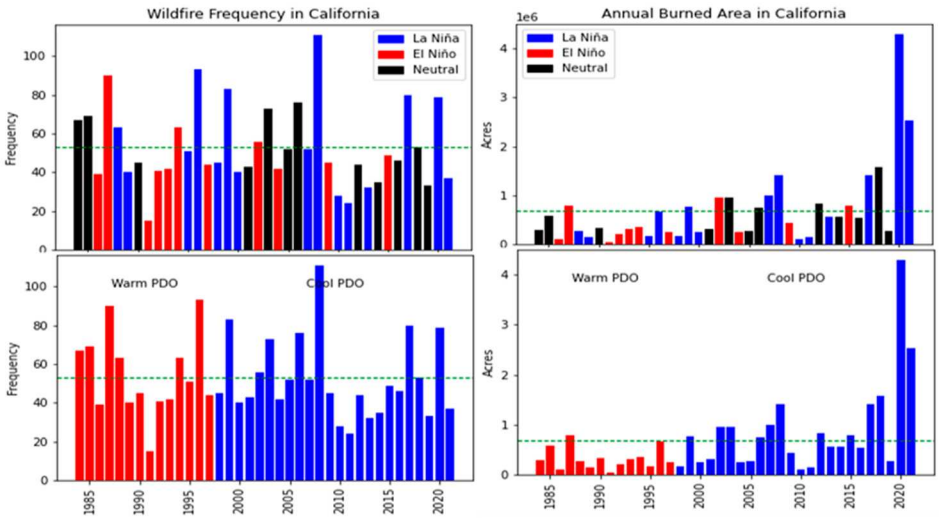

Figure 3. Year-to-year variability in CA wildfire frequency of occurrences (**left column**) and area burned in acres (**right column**). The top panels exhibit wildfires under El Niño (red), La-Niña (blue), and Neutral (black) environments. The bottom panels present wildfires under the PDO warm (red) and cool (blue) phases. The figures are for boreal summer (JJA). The green horizontal line delineates the average annual area burned or frequency of occurrences.

Increasing burned areas during the cool PDO phase is noteworthy. The cool phase is typically associated with cooler sea surface temperature anomalies along western North America in the eastern North Pacific and warmer sea surface temperature anomalies in the central North Pacific. These temperature patterns can result in lower sea level pressure along the northeast Pacific coast, affecting weather patterns across western North America [60]. During the summer, the cooler SST anomalies along the west coast promote reduced water vapor capacity in the atmosphere, and as such, produce drier air. Such a seemingly counter-intuitive condition suggests the complex nature of wildfire mechanisms over CA.

Next, we assessed annual wildfire occurrence for the partitioned R1, R2, and R3 regions (described in Section 2). Each region exhibits unique terrain and wildfire patterns and is dotted with rolling hills and deep valleys. The local terrain features have a strong control on flow patterns. This is revealed in Figure 4, which presents the summer interannual wildfire frequency over R1, R2, and R3.

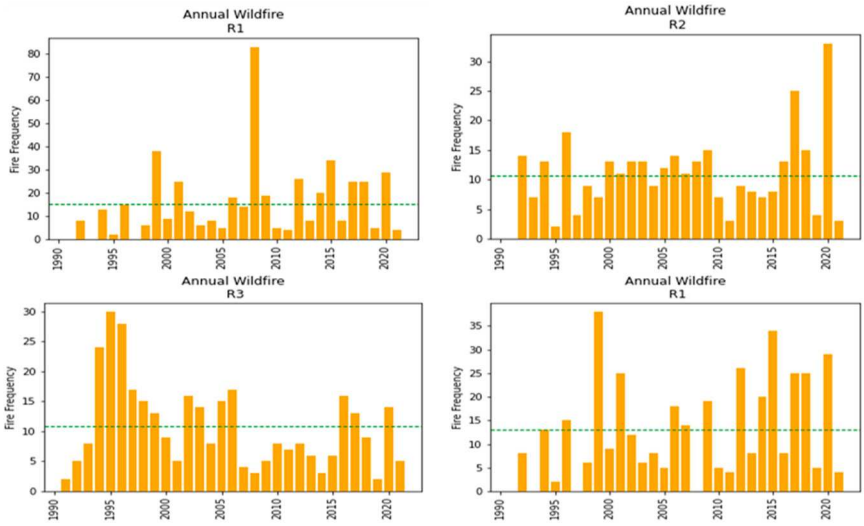

Figure 4. Annual frequency of wildfire occurrences during boreal summer (JJA). The green horizontal line delineates the average wildfire frequency for R1, R2, and R3 regions. An anomalously high frequency of wildfire is seen over R1. For comparative analysis, R1 is reproduced without 2008 in the bottom right panel. Regional data are available from 1991.

Above-average wildfire frequency is observed 35% of the time in R1, 51% of the time over R2, and 42% of the time over R3. We note that in R1, 80 wildfire events were observed in 2008. Because the 2008 anomalously high occurrence was in the R1 region only (Figures 3 and 4), we treated 2008 as an outlier, and as a result, we reproduced R1 without 2008 for the comparative analysis (Figure 4; lower right panel) in order to investigate wildfire patterns in each region.

The variability in wildfire activities across California's regions can be attributed to a combination of factors, including local topographic and climatic conditions, vegetation types, and anthropogenic influences.

As suggested in [61], in the R1 region, a series of dry lightning storms ignited most wildfires during the summer of 2008 [61]. The 2008 events coincided with a La-Niña phase during a cool PDO, and the combined effects reinforced each other and further exacerbated the fire risk. It is to be noted that the region's rugged topography, characterized by steep slopes and deep canyons, accelerated the spread of wildfires and could make wildfire management and firefighting efforts more challenging, and its nature may have contributed to the frequent occurrences. Additionally, R1 experienced a severe drought in the years leading up to 2008, resulting in low soil moisture and dry vegetation, which increased fire risk. According to the California Department of Water Resources (DWR), the water years 2007–2009 represented the 12th driest three-year period in recorded climatic history [62], creating ideal conditions for the ignition and spread of wildfires.

The combination of dry lightning storms [63], La-Niña conditions, a cool PDO phase, rugged topography, and severe drought [62] created a perfect storm for widespread wildfire activity in R1 during the summer of 2008.

Similar conditions were observed in R2 during the summer of 2020, resulting in the largest recorded wildfire in California's history. In August 2020, a series of lightning storms sparked hundreds of fires across R1 and R2, particularly in the Coast Ranges and the Sierra Nevada foothills. These fires, collectively known as the August Complex [63], burned over 1 million acres. The lightning storms occurred during a period of extreme heat, with record-breaking temperatures and low humidity [64], creating ideal conditions for fire ignition and spread.

3.2. Patterns of Moisture Deficit and FWI BSISO, ENSO, and PDO

This section presents moisture deficit and FWI patterns for climate variabilities at intraseasonal, interannual, and interdecadal scales (Figures 5–8).

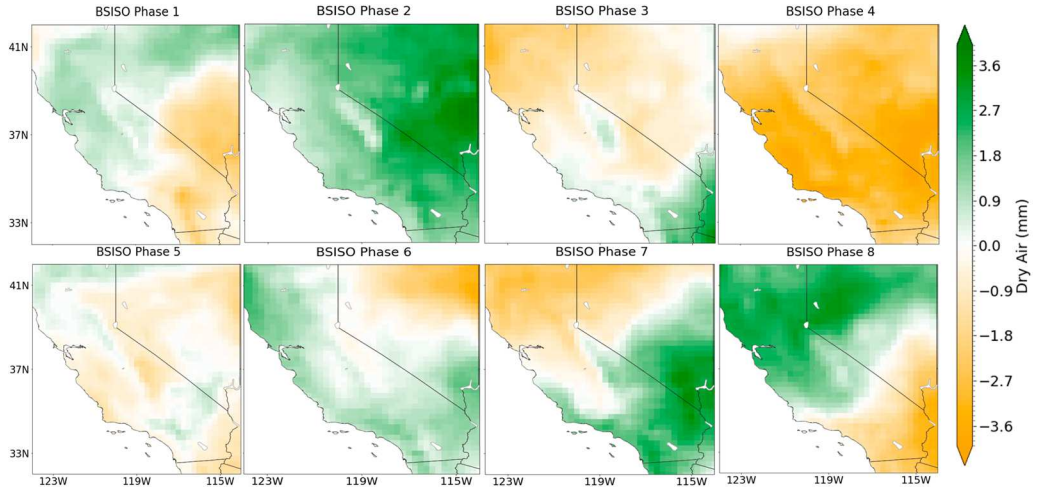

Figure 5. Composites of moisture deficit anomaly (mm) during BSISO phases (1–8). Orange color represents drier than normal, while green color represents wetter conditions.

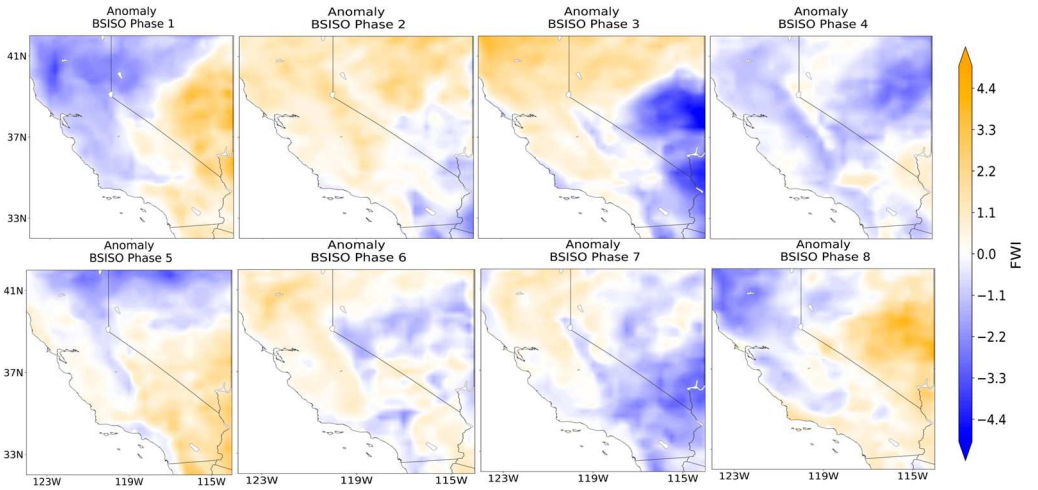

Figure 6. Same as Figure 5, except the figure shows the composites of fire weather index (FWI) anomalies.

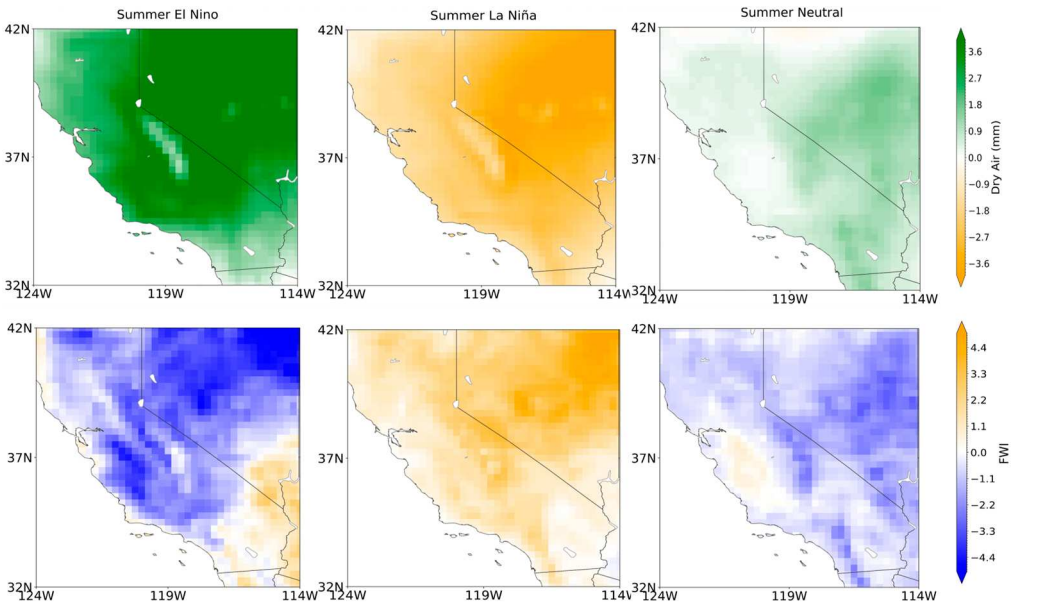

Figure 7. Anomaly composites of moisture deficit (mm) (**top panel**) and fire weather index (FWI) (**bottom panel**) during the ENSO phases; El Niño (**left column**), La-Niña (**middle column**), and Neutral

(**right column**). Anomalies are based on deviation of each ENSO phase from the combined JJA mean conditions for a period of 1980–2021.

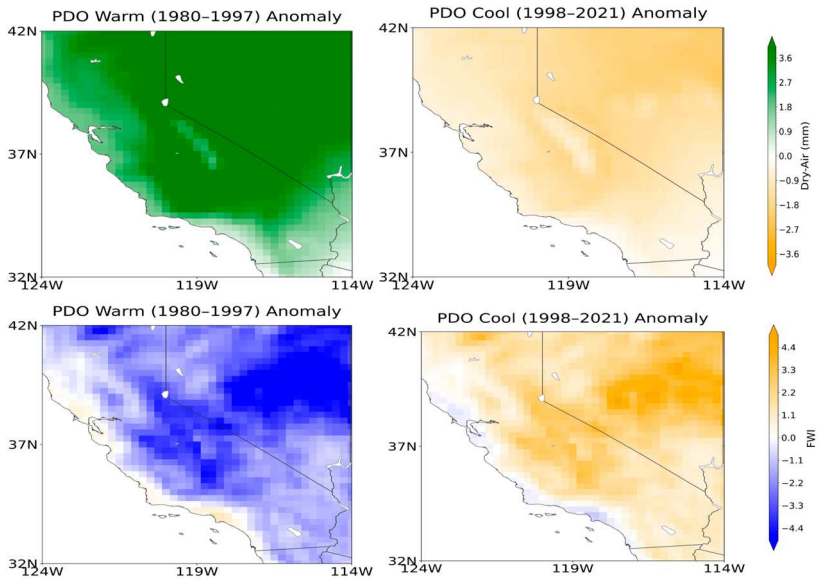

Figure 8. Anomaly composites of moisture deficit (mm) (**top**) and fire weather index (FWI) (**bottom**) during the PDO phases; warm (**left**) and cool (**right**). We calculated each parameter under cool (1998–2021) and warm (1980–1997).

3.2.1. The Boreal Summer Intraseasonal Oscillation (BSISO)

To investigate the effect of intraseasonal variability on wildfire dynamics, we began by analyzing the FWI and dry air anomalies related to BSISO. This was carried out using the BSISO index to determine the geographical position of the oscillation pattern (phase) and the strength of the oscillation (amplitude). Past work suggested that the BSISO plays an important role in the northward propagation of convection over the western North Pacific Ocean, which effects atmospheric circulation patterns and influences weather systems over a wider region, including California [26].

It is well documented that enhanced cloudiness and precipitation are associated with enhanced convective phases of the BSISO (for example, phases 1–2 are linked with increased convection and an unstable atmosphere over the northern Indian Ocean [25]). Studies (e.g., [61]) suggested that enhanced precipitation occurs over the west coast of the US when convective activity is stronger over the Indian Ocean [65].

We analyzed anomalies in dry air and the FWI by determining deviations from the June–August average over the 1980–2021 study period for each BSISO phase (Figures 5 and 6). Figure 5 presents composite dry air anomalies for the eight BSISO phases, where drier than normal air is represented by the orange shading.

Marked variability in the moisture content of the atmosphere is observed during the BSISO progression (Figure 5). In the shift from phase 2 to 3, we observed drier air, especially in Northern California, parts of the Central Coastal Ranges, and Death Valley. However, in phase 4, predominant dryness envelops the entire state of California, signifying a notable departure from mean moisture levels. The dry anomalies in phase 4 cover a larger spatial extent compared to the other phases, with most of California experiencing drier-than-normal conditions. This widespread aridity, resulting from fluctuation in atmospheric moisture linked to the BSISO's spatial–temporal evolution [66], sets the stage for heightened wildfire risk.

In the R1 region, there is a marked tendency for extremely dry conditions during BSISO phases 3, 4, and 7. The dry anomalies in R1 during these phases range from −1.8 to −3.6 mm, indicating significantly drier conditions compared to the average. This pattern

is most likely due to alterations in air circulation and moisture transportation that occur during these specific stages of the BSISO cycle. Such changes can include reduced humidity and increased aridity, laying the groundwork for these dry conditions. In the R2 region, severe dryness is seen during phase 4, with dry anomalies less than −3.6 mm, while moderate to light dryness is observed during phases 3, 5, and 7, with anomalies ranging from −0.9 to −2.7 mm. In the R3 region, drier conditions are observed during phases 1, 4, and 8, with dry anomalies being most pronounced in phase 4 (values less than −2.7 mm).

In Figure 6, the percentage anomaly of the FWI is presented, showing the variability in wildfire risk across the eight BSISO phases. The results show that the R1 and R2 regions experience increased wildfire risk, particularly in the Klamath Mountains of the R1 region during phase 3. As phase 4 moves over the region, the wildfire risk reduces in the entire state. However, during phase 5, the Coastal Ranges, Sierra Nevada Mountains, and parts of elevated Southern California all exhibit heightened wildfire risk. As the BSISO advances to phase 6, the R1 and R2 regions continue to exhibit positive FWI anomalies, indicating higher-than-normal fire risk. During phase 7, the elevated fire risk becomes more restricted to parts of the northern mountains. Progressing to phase 8, the southern coast experiences an increased potential for wildfires, as evidenced by the positive FWI anomalies in this region.

The BSISO adds another layer of complexity to the climatic interplay, such that its influence on moisture distribution and wildfire risks may vary from region to region [29]. While Northern California experiences drier-than-average conditions during phases 3, 4, and 7, the FWI anomalies do not always align with the dry air anomalies. For instance, in phase 4, despite the extremely dry conditions, the FWI anomalies indicate lower-than-average wildfire risk in Northern California. Conversely, during phase 2, when dry conditions are less pronounced, the FWI anomalies suggest higher-than-average wildfire risk in this region. Phase 4 shows a pronounced dry impact on California and parallels some studies that explored the atmospheric anomalies stemming from BSISO's evolution [26]. The regional complexity, particularly the distinct patterns in Northern and Southern California, highlights the interplay between large-scale climate drivers and local factors, a phenomenon also discussed by Nicholas et al. (2020) [67]. Their study examined the various drivers of wildfire severity and spatial variability in the 2013 Rim Fire in the Sierra Nevada mountain range in eastern California, highlighting the multi-scale nature of their influences. Recognizing the disparities in the effects of climatic oscillations across different regions can aid in developing more targeted preventive strategies in California.

3.2.2. ENSO

Figure 7 shows composites of dry air anomalies and FWI anomalies during ENSO phases. The orange color shows drier conditions and more proneness to wildfires. During the El Niño phase, there is a decrease in moisture deficit and FWI values. This observation supports the findings of Hoell et al. [68], who highlighted that during strong El Niño events, the easterly trade winds weaken or even reverse in the Pacific Ocean. This allows warm water to move eastward, increasing the SST in the eastern Pacific and leading to increased evaporation and higher chances of precipitation over California. Additionally, this finding is also in line with the results of Cole et al. [69], who found that during La-Niña events, significant dry periods were associated with decreased moisture due to the upwelling of cooler waters in the eastern Pacific. This phenomenon coincides with the strengthening of easterly trade winds across the Pacific Ocean during La-Niña episodes.

Our findings revealed a notable decrease in the moisture deficit (top panel) and FWI (bottom panel) during El Niño (left column). Previous research has shown that during a strong El Niño, CA is expected to be wetter than normal [15], reducing very large fires. Similarly, in the study region, the atmosphere exhibits increased moisture content, nearing a level that significantly lowers the likelihood of wildfires, as indicated by a decrease in the fire weather index (FWI). However, during the La-Niña phase (middle), we observed an increasing moisture deficit, indicating drier atmospheric conditions and an increased risk of

wildfires. These patterns are consistent with the typical climatological behavior associated with these phases: El Niño often brings about increased rainfall and wetter conditions [68], while La-Niña tends to usher in drier conditions [69].

3.2.3. Pacific Decadal Oscillation (PDO)

We now highlight the influence of the Pacific Decadal Oscillation (PDO) on moisture deficit and wildfire risk. Figure 8 presents the climatology of moisture deficit (top panels) and the fire weather index (FWI) (bottom panels) under different phases of the PDO. It is important to note that the anomalies depicted in the figure on the left are averaged during the most recent warm PDO period (1980–1997), while those on the right represent the current, predominately cool PDO phase (1998–2021). Wet conditions are observed during the warm PDO phase, while the cool PDO phase is associated with conditions that are drier than the long-term average. These dry conditions often result from variability in sea surface temperature patterns and subsequent atmospheric responses and may lead to decreased soil moisture and reduced surface humidity [70]. There are higher wildfire risks due to these dry circumstances, as depicted earlier (Figures 3 and 4), where we observed above-average wildfire conditions during the cool phase. Our study shows that the cool PDO is linked with increased wildfire potential and moisture below the mean condition. Not only is there less precipitation, but there may be more accessible fuel owing to parched vegetation, which further increases wildfire risk.

The PDO's influence on drought and wildfire propensity, as depicted in this study, is consistent with the observations of Schoennagel et al. [14]. Schoennagel et al. noted that almost 70% of significant wildfires in the southern Rockies occurred during a combination of La-Niña and negative PDO phase. Their study over the Rocky Mountains showed that the PDO, especially when considered in conjunction with ENSO phases, plays a significant role in influencing drought-induced wildfires, which is consistent with our study. However, the impact of the co-occurrence of BSISO phases with cool or warm phases of the PDO on wildfire risks has not yet been demonstrated.

3.3. An Analysis of Wildfire Risk under Combined PDO and BSISO Conditions

We have shown the effects of individual large-scale conditions on wildfire risk; we now investigate the combined effect of PDO and BSISO. This exploration is crucial since longer-term teleconnections like PDO can influence intraseasonal changes in fire weather conditions and modulate the effect of seasonal to intraseasonal oscillation/teleconnections (e.g., BSISO and ENSO), an area still under-researched.

Figure 9 presents the FWI anomalies for each BSISO phase during the recent cool PDO period (1998 to 2021). Figure 10 presents the FWI anomalies for each BSISO phase within the warm PDO period from 1980 to 1997. The plots illustrate the anomalies of the FWI for each BSISO phase, indicating the deviations of the FWI from the average conditions throughout the cool or warm PDO. The purpose of this analysis is to investigate the conditions associated with different BSISO phases under the influence of the warm or cool PDO and to compare them with those observed when considering the BSISO independently.

During the warm PDO period, BSISO phase 2 is characterized by a persistent positive sea surface temperature anomaly across the equatorial Pacific Ocean and a simultaneous negative anomaly in the central northern Pacific Ocean. The interaction between these anomalies and the atmospheric and climatic conditions typical of BSISO phase 2 results in a substantial increase in wildfire risk conditions (Figure 10). In contrast, during the cool PDO phase, which features negative sea surface temperature anomalies along the equatorial Pacific, there is a significant reduction (Figure 9) in the conditions that usually enhance wildfire risks during BSISO phase 2. The cooler ocean temperatures and the associated atmospheric patterns tend to mitigate or weaken the typical influences of this BSISO phase, resulting in more subdued or less pronounced FWI patterns.

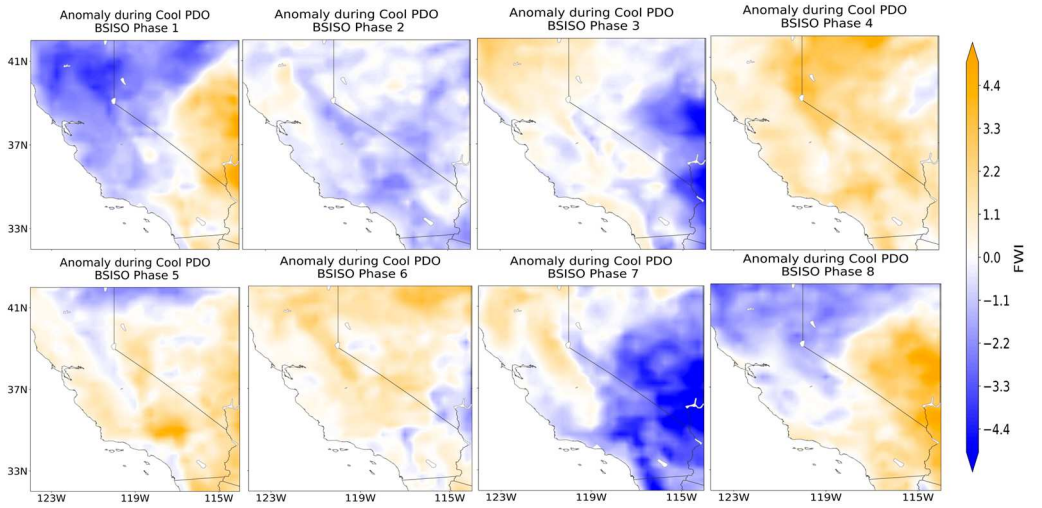

Figure 9. The 1998–2021 composites of FWI anomalies during each BSISO phase of cool PDO only.

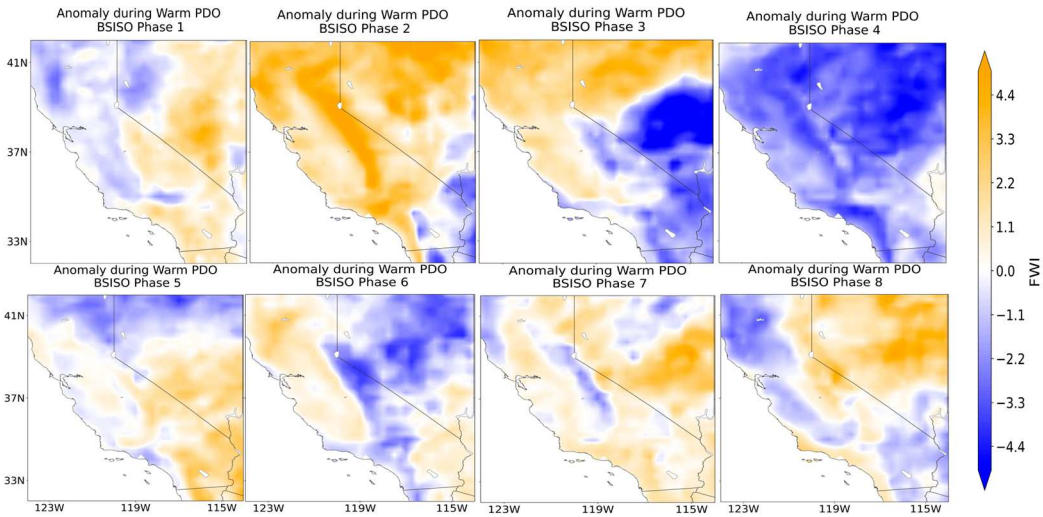

Figure 10. Same as Figure 9, except under the warm PDO period (1980–1997).

The cool phase of the PDO is generally associated with drier conditions in California (see Figure 8). During BSISO phases 1, 7, and 8, we observed a negative anomaly that counteracts the typically dry signal from cool PDO and La-Niña phases. These BSISO phases appear to reduce fire weather risk in R1 and R2 during phases 1 and 8, and in region R3 during phase 7.

Moreover, the impact of the co-existence of the cool PDO with the BSISO is evident in phase 2 across the Sierra Nevada and southern mountain regions. Initially, when examining the BSISO independently, positive FWI anomalies were observed in regions R1 and R2, with only a weak positive anomaly in parts of R3. However, during the cool PDO phase, these anomalies transition toward normal to negative values, indicating a diminished wildfire risk.

In Figure 9, phases 1, 4, and 8 of the BSISO show contrasting results between the cool PDO phase and when the BSISO phases occur independently of the PDO cycle (Figure 6). During phases 1 and 8, the cool PDO phase exhibits more pronounced negative anomalies compared to when these BSISO phases operate alone. This is particularly evident in areas such as the Sierra Nevada and the Northern California mountains, where the interaction between phases 1 and 8 of the BSISO and the cool PDO appears to suppress the wildfire risk more than when these BSISO phases occur independently.

However, during phase 4, the relationship between the BSISO and the cool PDO phase is notably different. In Figure 6, phase 4 is characterized by a lower-than-average FWI (blue

shading) across most of California. In contrast, Figure 9, which represents the cool PDO phase, exhibits a strongly higher-than-average FWI (dark orange shading) in R1. This stark difference suggests that the interaction between BSISO phase 4 and the cool PDO amplifies the wildfire risk in R1, as opposed to the suppressing effect observed in phases 1 and 8.

The findings reveal that the conditions experienced during each BSISO phase vary between the cool and warm PDO periods. Interestingly, there is a reversal in the sign of anomalies in the Sierra Nevada Mountains during BSISO phases 1, 2, 4, and 8. A comparison of the FWI anomalies associated with the independent occurrence of the BSISO (Figure 6) and those during the warm PDO (Figure 10) shows that BSISO phases 1, 2, 3, and 8 intensify the potential for wildfires in the R1 region. Furthermore, phase 6 is associated with an increased wildfire potential in the Klamath Mountains region.

Wildfire risk is reduced across all regions of California during BSISO phase 4. Moreover, this reduction in wildfire risk persists into BSISO phases 5, 6, and 7 in areas that already exhibit negative anomalies, as indicated by the FWI data. In summary, during the cool PDO, wildfire risks in the R1 region are reduced during all BSISO phases except phase 4, when they are enhanced. In R2, wildfire risks are mostly suppressed during BSISO phases 1 to 3 and 6 to 8, enhanced during phases 4, and near normal during phase 5. Finally, in R3, wildfire risks are suppressed during phases 1, 2, 5, 7, and 8, enhanced during phases 4, and near normal during phases 3 and 6.

In summary, during the cool PDO, wildfire risks in the R1 region are reduced during all BSISO phases except phase 4, when they are enhanced. In R2, wildfire risks are mostly suppressed during BSISO phases 1 to 3 and 6 to 8, enhanced during phases 4, and near normal during phase 5. Finally, in R3, wildfire risks are suppressed during phases 1, 2, 5, 7, and 8, enhanced during phases 4, and near normal during phases 3 and 6.

Consistent with previous studies (e.g., [14]), the results in this study suggest that the PDO can enhance or suppress the characteristics of specific BSISO phases, thereby influencing FWI patterns. It is important to note that while our study focuses on the combined effect of PDO and BSISO on wildfire risk, the potential interaction between PDO, ENSO, and BSISO should be considered. Furthermore, the possibility of a closer relationship between BSISO and ENSO warrants further investigation.

3.4. Synoptic to Large-Scale Impact on Moisture, Temperature, and Wildfire Risk

In this section, we explore how the FWI is influenced by moisture conditions, utilizing both relative humidity (RH) and vapor pressure deficit (VPD) as indicators. While RH quantifies the moisture level in the atmosphere relative to its maximum capacity at a given temperature, VPD measures the atmospheric moisture demand independent of temperature. Both metrics play distinct roles in assessing wildfire risk through the FWI.

RH offers insights into the ambient air moisture, which directly affects the moisture content of dead and live fuel. Lower RH values indicate drier air, leading to increased evaporative demand and faster drying of fuels, thereby increasing the overall wildfire potential. As evident from the strong negative correlation between the FWI and RH (left column, Figure 11), areas with lower RH exhibit higher FWI values and, consequently, elevated wildfire risk.

On the other hand, VPD provides information on the potential for moisture loss from vegetation and soil due to the atmospheric moisture demand. Higher VPD corresponds to drier vegetation and soil, increasing the availability of dry fuel for wildfires. The strong positive correlation between the FWI and VPD (right column, Figure 11) in the R1 and R2 regions and coastal mountains in R3 highlights how elevated VPD is associated with an increased risk of wildfires in these areas.

It is important to note that in the desert region of R3, correlations between the FWI and VPD are weak or not significant. This can be attributed to the lack of vegetation in these arid areas, where fuel availability is limited, making the region less susceptible to wildfire risk despite potential changes in VPD.

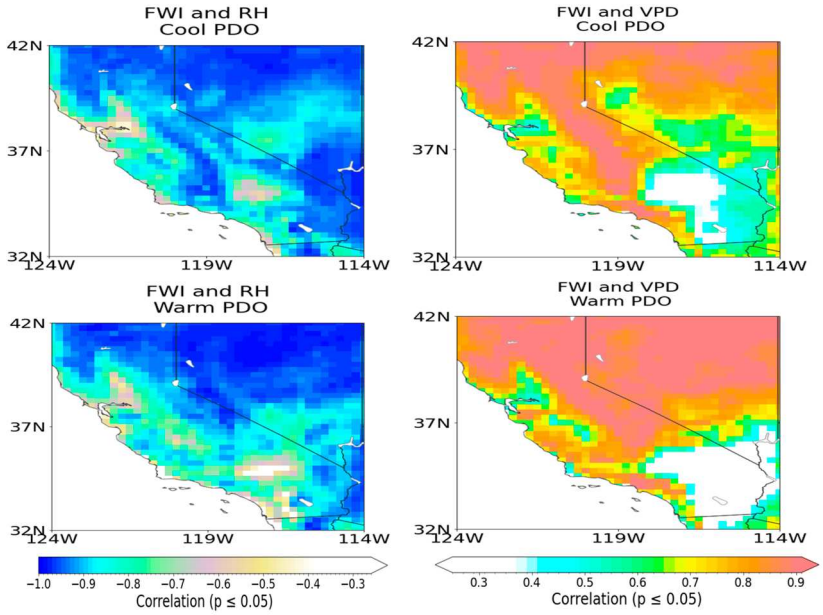

Figure 11. Correlation between the FWI and RH (%) (**left column**) and the FWI and VPD (kPa) (**right column**) during the cool (**top panel**) and warm (**bottom panel**) PDO phases.

While both RH and VPD contribute to the FWI's assessment of wildfire risk, they capture distinct aspects of the moisture dynamics influencing fuel conditions. RH directly reflects the moisture content of fuels, while VPD indicates the potential for further drying of fuels due to atmospheric moisture demand. Together, these metrics provide a comprehensive understanding of the complex interplay between atmospheric conditions and wildfire risk, as reflected in the strong correlations with the FWI across different climatic phases.

Next, we examined the relationship between 2 m temperature and the FWI during the ENSO and PDO phases across the regions. Figure 12 presents the correlation between the FWI and temperature during the PDO phases (left), cool PDO (top) and warm PDO (bottom), and during the ENSO phases (right), La-Niña (top) and El Niño (bottom). Strong positive correlations are observed in the northern mountains and Sierra Nevada mountains of R1 and R2, while R3 shows no correlations except along the coastlines. As previously stated, the deserts in R3 are characterized by low fuel due to sparse vegetation and very low winds, and they exhibit no correlations. This reflects the reduced wildfire risk despite potential temperature increases. This aligns with the understanding that lower fuel availability in these arid regions significantly mitigates the likelihood of wildfires, even under warmer conditions. Conversely, along the coastlines in the R3 region, the strong positive correlation can be attributed to higher vegetation density, which provides more fuel, especially after a winter with increased precipitation, and when coupled with increased temperatures, wildfire risk is elevated.

Our findings show that during the PDO phases, the relationship between the FWI and temperature becomes more prominent, particularly in elevated regions. Mountainous regions often have unique microclimates, where temperature variations can significantly impact vegetation dryness and, consequently, wildfire risks.

In Figure 13, we observe the correlation between the FWI and RH during the phases of the BSISO. The correlation patterns vary significantly across the different BSISO phases and regions of California.

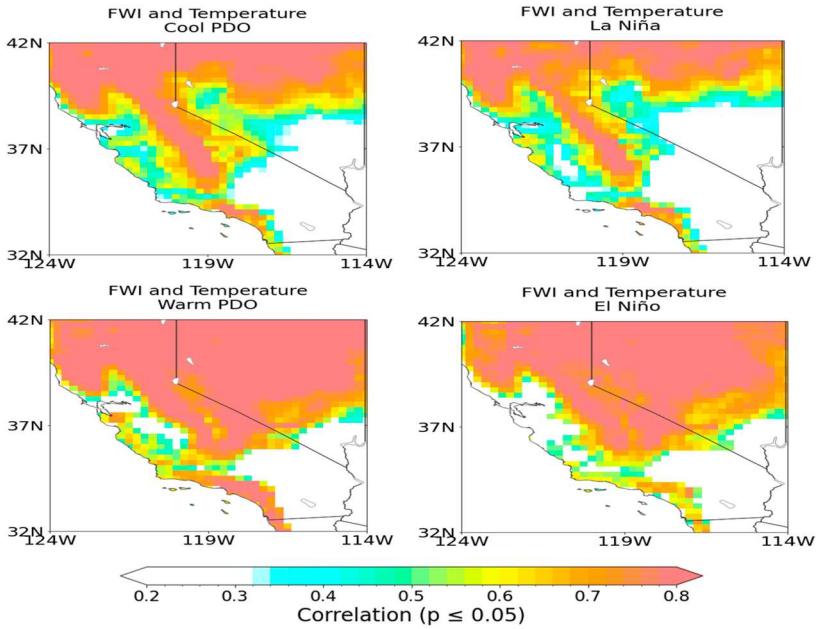

Figure 12. Correlation between FWI and 2 m temperature (°C) during cool (**top**) and warm (**bottom**) PDO (**left**) and La-Niña (**top**) and El Niño (**bottom**) ENSO (**right**) phases. Dark orange shading represents strong positive correlation.

During phases 1 and 8, a very strong negative correlation between the FWI and RH is evident in the northern and central regions of California, particularly in the Klamath Mountains, southern Cascade Range, and Sierra Nevada. This strong negative correlation indicates that a decrease in relative humidity is strongly associated with an increase in wildfire potential in these mountainous areas during these phases. The Coastal Ranges and the Central Valley also show a linear relationship between the variables, although not as strong as in the previously mentioned areas.

The Sierra Nevada Mountains, a crucial region for California's water resources and biodiversity, consistently show strong to very strong negative correlations throughout all BSISO phases. This persistent strong correlation suggests that Sierra Nevada is particularly sensitive to changes in relative humidity, with lower humidity levels consistently leading to higher wildfire potential. The strong relationship between the FWI and RH in Sierra Nevada highlights the importance of monitoring and managing this region during the fire season, as it may be more prone to wildfire outbreaks under favorable conditions.

In contrast, a weaker linear relationship is observed along the Sacramento Valley and parts of the San Joaquin Valley during phases 2, 3, and 7. This suggests that the influence of relative humidity on wildfire potential is less pronounced in these regions during these specific BSISO phases.

The Klamath and Cascade Mountains also exhibit strong to very strong negative correlations throughout the BSISO phases, indicating that these regions are similarly sensitive to changes in relative humidity and have higher wildfire potential when humidity levels decrease.

In summary, the correlation analysis reveals that the Sierra Nevada, Klamath, and Cascade Mountains are the most sensitive to changes in relative humidity, consistently showing strong to very strong negative correlations with the FWI across all BSISO phases. This finding emphasizes the need for heightened wildfire monitoring and management efforts in these regions, particularly during periods of low relative humidity. The spatial and temporal variability in the relationship between FWI and RH across California also underscores the importance of considering regional differences and BSISO phases when assessing and mitigating wildfire risks.

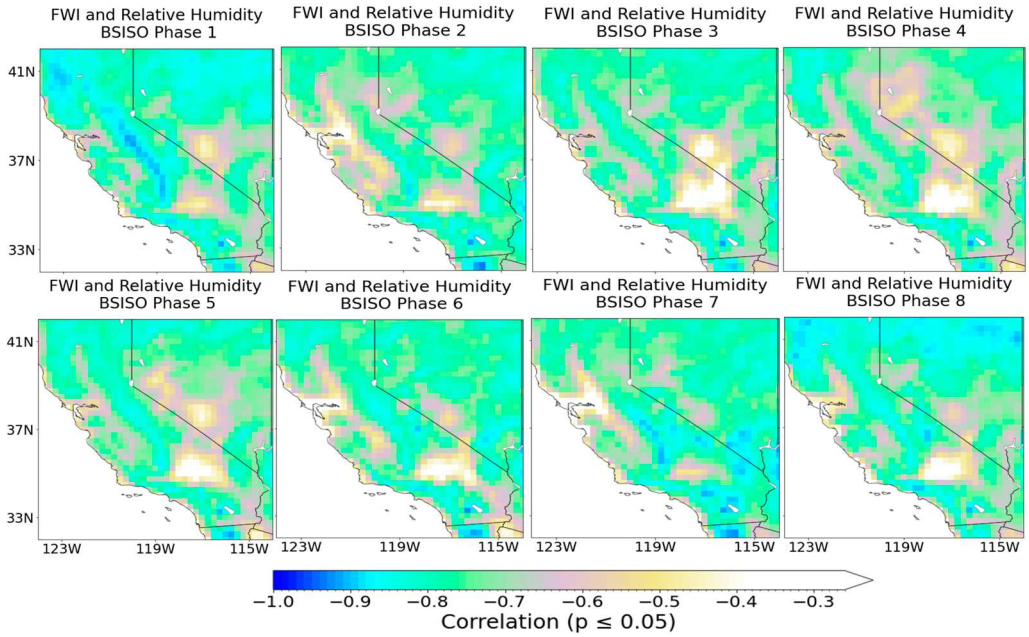

Figure 13. Correlation between FWI and RH (%) during the BSISO phases. Shaded areas are statistically significant.

While our study has uncovered significant correlations between meteorological factors, teleconnections, and wildfire occurrence in California, it is essential to acknowledge the limitations of relying solely on correlation-based analysis. Correlation does not necessarily imply causation, and there are potential pitfalls in inferring causal relationships from such associations [71]. However, we argue that our conclusions remain robust despite the absence of a formal causal analysis. First, the physical mechanisms linking meteorological conditions and wildfire occurrence are well established in the literature (e.g., [72]). These studies have demonstrated that factors such as temperature and moisture play a crucial role in determining fuel moisture content and fire behavior. Second, the consistency of our findings across multiple regions and time scales suggests that the observed relationships are not merely spurious correlations but are likely indicative of underlying causal processes.

Furthermore, our results align with previous research that has identified similar connections between large-scale climate patterns and wildfire activity in California (e.g., [12,73]. While these studies also rely primarily on correlation-based analysis, they provide valuable context and support for the validity of our conclusions.

Nevertheless, we acknowledge that future research employing more advanced causal inference techniques, such as those described in [74], could help to strengthen the causal claims made in this study.

4. Conclusions and Final Remarks

This study investigates the impacts of climate patterns, such as ENSO, PDO, and BSISO, on wildfire risk and behavior in the wildfire-prone region of California.

The La-Niña phase of ENSO and the cool phase of PDO are found to be associated with reduced atmospheric moisture and higher air temperatures, intensifying drought conditions. On the other hand, the El Niño phase and warm PDO are linked to increased atmospheric moisture, which can mitigate immediate wildfire risks but may contribute to long-term wildfire potential through the vegetation growth and subsequent drying. Additionally, during the BSISO's progression, significant variability in atmospheric moisture is observed across its phases, profoundly impacting California's moisture content. From phase 2 to 3, a notable decrease in humidity is seen, particularly affecting Northern California, the Central Coastal Ranges, and Death Valley. This dryness intensifies during phase 4, where nearly all of California experiences significantly drier-than-usual conditions,

showing the most extensive dry anomalies. Such widespread aridity due to BSISO-related atmospheric changes notably heightens the state's wildfire risk. In more detail, the R1 region (Northern California) experiences severe dryness during phases 3, 4, and 7, with dry anomalies ranging significantly above average, suggesting profound changes to moisture transport. In the R2 region (Central California), phase 4 brings severe dryness, markedly exceeding typical conditions, while phases 3, 5, and 7 show moderate to light dryness. Similarly, the R3 region (Southern California) sees its driest conditions during phases 1, 4, and 8, with the most extreme dryness occurring in phase 4.

The interaction between the PDO and BSISO phases has a complex and region-specific effect on fire weather conditions. PDO enhances or suppresses the fire weather conditions of BSISO phases, thereby influencing FWI patterns. During the cool PDO, BSISO phases 1, 7, and 8 are characterized by a marked reduction in wildfire risk across various regions of California. This trend is particularly pronounced in the R1 (Northern California) and R2 regions (Central California) for phases 1 and 8 and in the R3 region (Southern California) for phase 7, highlighting the cool PDO's significant role in dampening conditions conducive to wildfires. The influence of the cool PDO also extends to BSISO phase 2, covering the Sierra Nevada and southern mountains, where it moderates FWI anomalies from positive towards neutral or negative. This modification indicates a reduced wildfire risk, contrasting sharply with scenarios where the BSISO functions independently, showing positive FWI anomalies in the R1 and R2 regions. The differences between the cool PDO and BSISO phases operating alone are particularly noticeable in phases 1, 4, and 8. In phases 1 and 8, the cool PDO enhances the negative FWI anomalies, indicating a stronger suppression of wildfire risks compared to when these phases occur without the influence of the PDO. However, phase 4 presents a distinct scenario under the cool PDO, and rather than a decrease, there is a significant increase in wildfire risk in the R1 region, as indicated by marked higher FWI anomalies. This represents a clear deviation from the suppression of wildfire risks typically observed in other phases under the cool PDO. During the warm PDO period, BSISO phases 1, 2, 3, and 8 intensify the potential for wildfires in the northern region of California (R1), with phase 6 increasing the risk in the Klamath Mountains. Furthermore, wildfire risk is diminished across all regions of California during BSISO phase 4, with this reduction persisting into phases 5, 6, and 7 in areas already exhibiting negative FWI anomalies.

The study shows that the fire weather index (FWI), relative humidity (RH), vapor pressure deficit (VPD), and temperature are closely intertwined and serve as crucial indicators of wildfire risk in California. Lower RH and higher VPD values are strongly correlated with increased FWI, signifying higher wildfire potential. Temperature also plays a vital role, particularly in mountainous regions like the Sierra Nevada, Klamath, and Cascade Mountains, where variations can substantially influence fuel moisture content and, consequently, wildfire potential. These mountainous areas have unique microclimates where temperature variations can significantly impact vegetation dryness, and the relationship between the FWI and temperature becomes more prominent during the PDO phases. Furthermore, the Sierra Nevada, Klamath, and Cascade Mountains consistently exhibit a strong linear relationship between the FWI and RH throughout all phases of the BSISO, indicating that these regions are highly sensitive to changes in RH, regardless of the BSISO phase.

The relationship between FWI and climatic factors like temperature and moisture content varies geographically within California. In elevated regions, such as the Sierra Nevada, Klamath, and Cascade Mountains, there is a strong positive correlation between the FWI and temperature ($r > 0.7$, $p \leq 0.05$). The study also emphasizes the complex interaction between California's diverse topography and wildfire behavior, especially the significant role of strong downslope winds, such as the Santa Ana winds, in exacerbating wildfire conditions. Elevated areas, like the Sierra Nevada Mountains, are particularly susceptible to temperature variations which can lead to heightened wildfire risks when combined with large-scale climatic influences. Along the Sierra Nevada Mountains, there is a strong negative correlation between the FWI and relative humidity ($r \leq -0.7$, $p \leq 0.05$). This

indicates that these regions are highly sensitive to changes in relative humidity, with lower humidity levels consistently leading to higher wildfire potential. In the Sacramento Valley and parts of the San Joaquin Valley, the influence of relative humidity on wildfire potential is less pronounced during specific BSISO phases, suggesting that the relationship between the FWI and relative humidity varies depending on the region and the prevailing BSISO phase. In the desert regions of Southern California (R3), there is a weak or non-significant correlation between FWI and VPD, primarily due to the area's lack of vegetation, which makes it less susceptible to wildfire risk despite potential temperature increases. These geographical variations in the relationship between the FWI and climatic factors, along with the influence of topography and local wind patterns, emphasize the importance of region-specific wildfire risk assessments and management strategies that take into account local climatic and topographic conditions. Understanding these regional differences is crucial for developing effective wildfire prevention, preparedness, and response measures across California.

Our study provided information based on current climate, which will be valuable for long-term wildfire risk management and considerations of climate change adaptation strategies. We recommend that future research should also focus on incorporating additional variables, such as land use changes and human activities, to develop more comprehensive wildfire risk assessment tools. Another potential direction for future research is the use of coupled global climate models (GCMs) that incorporate fire models, as demonstrated by [75]. These integrated modeling frameworks allow for a more comprehensive exploration of the feedback loops between climate, vegetation, and wildfire.

In conclusion, this study provides a comprehensive analysis of the complex interactions between large-scale climate oscillations, drought conditions, temperature fluctuations, and wildfire dynamics in California. The findings highlight the importance of considering the interplay between these factors and the geographical variations in wildfire risk assessment across the state. By advancing our understanding of these relationships, this research contributes to the development of more effective wildfire management strategies and climate change adaptation efforts in California.

Author Contributions: S.A. contributed to writing and computation, including visualization. B.G. contributed to writing. A.M. and Y.-L.L. contributed to writing, funding acquisition, and conceptualization. All authors have read and agreed to the published version of the manuscript.

Funding: This research was funded by the National Science Foundation (NSF) RISE under grant number 2022961. Afolayan was partially supported by the NSF Wildfire award under grant number 1900621.

Institutional Review Board Statement: Not Applicable.

Informed Consent Statement: Not Applicable.

Data Availability Statement: Data processed and used, including production scripts, can be made available upon request.

Acknowledgments: The authors acknowledge Argonne National Laboratory for their support of computing time on the Bebop supercomputer.

Conflicts of Interest: The authors declare no conflicts of interest.

References

1. Westerling, A.L. Increasing western US forest wildfire activity: Sensitivity to changes in the timing of spring. *Philos. Trans. R. Soc. B Biol. Sci.* **2016**, *371*, 20150178. [CrossRef] [PubMed]
2. Keeley, J.E.; Syphard, A.D. Twenty-first century California, USA, wildfires: Fuel-dominated vs. wind-dominated fires. *Fire Ecol.* **2019**, *15*, 24. [CrossRef]
3. Littell, J.S.; Peterson, D.L.; Riley, K.L.; Liu, Y.; Luce, C.H. A review of the relationships between drought and forest fire in the United States. *Glob. Chang. Biol.* **2016**, *22*, 2353–2369. [CrossRef] [PubMed]
4. Scasta, J.D.; Weir, J.R.; Stambaugh, M.C. Droughts and Wildfires in Western U.S. Rangelands. *Rangelands* **2016**, *38*, 197–203. [CrossRef]

5. Newcomer, M.E.; Underwood, J.; Murphy, S.F.; Ulrich, C.; Schram, T.; Maples, S.R.; Peña, J.; Siirila-woodburn, E.R.; Trotta, M.; Jasperse, J.; et al. Prolonged Drought in a Northern California Coastal Region Suppresses Wildfire Impacts on Hydrology. *Water Resour. Res.* **2023**, *59*, e2022WR034206. [CrossRef]
6. Bin, C.; Yufang, J.; Erica, S.; Max, A.M.; Michael, L.G.; James, T.R. Climate, Fuel, and Land Use Shaped the Spatial Pattern of Wildfire in Californias Sierra Nevada. *J. Geophys. Res. Biogeosci.* **2021**, *126*, e2020JG005786.
7. Keeley, J.E.; Syphard, A.D. Historical patterns of wildfire ignition sources in California ecosystems. *Int. J. Wildland Fire* **2018**, *27*, 781. [CrossRef]
8. Dong, L.; Leung, L.R.; Qian, Y.; Zou, Y.; Song, F.; Chen, X. Meteorological Environments Associated with California Wildfires and Their Potential Roles in Wildfire Changes during 1984–2017. *Geophys. Res. Atmos.* **2021**, *126*, e2020JD033180. [CrossRef]
9. Shabbar, A.; Skinner, W.; Flannigan, M.D. Prediction of Seasonal Forest Fire Severity in Canada from Large-Scale Climate Patterns. *J. Appl. Meteorol. Climatol.* **2011**, *50*, 785–799. [CrossRef]
10. Macias-Fauria, M.; Johnson, E.A. Large-scale climatic patterns control large lightning fire occurrence in Canada and Alaska forest regions. *J. Geophys. Res. Biogeosci.* **2006**, *111*, G04008. [CrossRef]
11. Keeley, J.E.; Syphard, A.D. Different historical fire–climate patterns in California. *Int. J. Wildland Fire* **2017**, *26*, 253–268. [CrossRef]
12. Keeley, J.; Syphard, A. Climate Change and Future Fire Regimes: Examples from California. *Geosciences* **2016**, *6*, 37. [CrossRef]
13. Fasullo, J.T.; Otto-Bliesner, B.L.; Stevenson, S. ENSO's Changing Influence on Temperature, Precipitation, and Wildfire in a Warming Climate. *Geophys. Res. Lett.* **2018**, *45*, 9216–9225. [CrossRef]
14. Schoennagel, T.; Veblen, T.T.; Romme, W.H.; Sibold, J.S.; Cook, E.R. ENSO and PDO variability affect drought-induced fire occurrence in Rocky Mountain subalpine forests. *Ecol. Appl.* **2005**, *15*, 2000–2014. [CrossRef]
15. Barbero, R.; Abatzoglou, J.T.; Brown, T.J. Seasonal reversal of the influence of El Niño-Southern Oscillation on very large wildfire occurrence in the interior northwestern United States. *Geophys. Res. Lett.* **2015**, *42*, 3538–3545. [CrossRef]
16. Krueger, E.S.; Levi, M.R.; Achieng, K.O.; Bolten, J.D.; Carlson, J.D.; Coops, N.C.; Holden, Z.A.; Magi, B.I.; Rigden, A.J.; Ochsner, T.E. Using soil moisture information to better understand and predict wildfire danger: A review of recent developments and outstanding questions. *Int. J. Wildland Fire* **2022**, *32*, 111–132. [CrossRef]
17. Huang, X.; Stevenson, S. Contributions of Climate Change and ENSO Variability to Future Precipitation Extremes over California. *Geophys. Res. Lett.* **2023**, *50*, e2023GL103322. [CrossRef]
18. Halofsky, J.E.; Peterson, D.L.; Harvey, B.J. Changing wildfire, changing forests: The effects of climate change on fire regimes and vegetation in the Pacific Northwest, USA. *Fire Ecol.* **2020**, *16*, 4. [CrossRef]
19. Harrison, M.; Meindl, C.F. A Statistical Relationship between El Niño-Southern Oscillation and Florida Wildfire Occurrence. *Phys. Geogr.* **2001**, *22*, 187–203. [CrossRef]
20. Goodrick, S.L.; Hanley, D.E. Florida wildfire activity and atmospheric teleconnections. *Int. J. Wildland Fire* **2009**, *18*, 476–482. [CrossRef]
21. Kipfmueller, K.F.; Larson, E.R.; St. George, S. Does proxy uncertainty affect the relations inferred between the Pacific Decadal Oscillation and wildfire activity in the western United States? *Geophys. Res. Lett.* **2012**, *39*, L04703. [CrossRef]
22. Kitzberger, T.; Brown, P.M.; Heyerdahl, E.K.; Swetnam, T.W.; Veblen, T.T. Contingent Pacific-Atlantic Ocean influence on multicentury wildfire synchrony over western North America. *Proc. Natl. Acad. Sci. USA* **2007**, *104*, 543–548. [CrossRef] [PubMed]
23. Gedalof, Z.; Peterson, D.L.; Mantua, N.J. Atmospheric, climatic, and ecological controls on extreme wildfire years in the northwestern United States. *Ecol. Appl.* **2005**, *15*, 154–174. [CrossRef]
24. Abatzoglou, J.T.; Brown, T.J. Influence of the Madden–Julian Oscillation on Summertime Cloud-to-Ground Lightning Activity over the Continental United States. *Mon. Weather Rev.* **2009**, *137*, 3596–3601. [CrossRef]
25. Zhang, C. Madden-Julian Oscillation. *Rev. Geophys.* **2005**, *43*, RG2003. [CrossRef]
26. Kikuchi, K. The Boreal Summer Intraseasonal Oscillation (BSISO): A Review. *J. Meteorol. Soc. Jpn.* **2021**, *99*, 933–972. [CrossRef]
27. Higgins, R.; Shi, W. Intercomparison of the principal modes of interannual and intraseasonal variability of the North American Monsoon System. *J. Clim.* **2001**, *14*, 403–417. [CrossRef]
28. Lorenz, D.J.; Hartmann, D.L. The Effect of the MJO on the North American Monsoon. *J. Clim.* **2006**, *19*, 333–343. [CrossRef]
29. Chen, G.; Wang, B. Diversity of the Boreal Summer Intraseasonal Oscillation. *JGR Atmos.* **2021**, *126*, e2020JD034137. [CrossRef]
30. Hunt, K.M.R.; Turner, A.G. Nonlinear intensification of monsoon low pressure systems by the BSISO. *Weather Clim. Dyn.* **2022**, *3*, 1341–1358. [CrossRef]
31. Huang, Y.; Wu, S.; Kaplan, J.O. Sensitivity of global wildfire occurrences to various factors in the context of global change. *Atmos. Environ.* **2015**, *121*, 86–92. [CrossRef]
32. Madadgar, S.; Sadegh, M.; Chiang, F.; Ragno, E.; AghaKouchak, A. Quantifying increased fire risk in California in response to different levels of warming and drying. *Stoch. Environ. Res. Risk Assess.* **2020**, *34*, 2023–2031. [CrossRef]
33. Meyn, A.; White, P.S.; Buhk, C.; Jentsch, A. Environmental drivers of large, infrequent wildfires: The emerging conceptual model. *Prog. Phys. Geogr.* **2007**, *31*, 287–312. [CrossRef]
34. Hayasaka, H.; Tanaka, H.L.; Bieniek, P.A. Synoptic-scale fire weather conditions in Alaska. *Polar Sci.* **2016**, *10*, 217–226. [CrossRef]
35. Zhong, S.; Yu, L.; Heilman, W.E.; Bian, X.; Fromm, H. Synoptic weather patterns for large wildfires in the northwestern United States—A climatological analysis using three classification methods. *Theor. Appl. Clim.* **2020**, *141*, 1057–1073. [CrossRef]
36. Brody-Heine, S.; Zhang, J.; Katurji, M.; Pearce, H.G.; Kittridge, M. Wind vector change and fire weather index in New Zealand as a modified metric in evaluating fire danger. *Int. J. Wildland Fire* **2023**, *32*, 872–885. [CrossRef]

37. Smith, C.; Hatchett, B.; Kaplan, M. A Surface Observation Based Climatology of Diablo-LikeWinds in California's Wine Country and Western Sierra Nevada. *Fire* **2018**, *1*, 25. [CrossRef]
38. Mass, C.F.; Ovens, D. The Synoptic and Mesoscale Evolution Accompanying the 2018 Camp Fire of Northern California. *Bull. Am. Meteorol. Soc.* **2021**, *102*, E168–E192. [CrossRef]
39. Carvalho, L.M.V.; Duine, G.; Jones, C.; Zigner, K.; Carvalho, L.; Duine, G.; Jones, C.; Zigner, K.; Clements, C.; Kane, H.; et al. The Sundowner Winds Experiment (SWEX) Pilot Study: Understanding Downslope Windstorms in the Santa Ynez Mountains, Santa Barbara, California. *Mon. Weather. Rev.* **2020**, *148*, 1519–1539. [CrossRef]
40. Di Giuseppe, F.; Vitolo, C.; Krzeminski, B.; Barnard, C.; Maciel, P.; San-Miguel, J. Fire Weather Index: The skill provided by the European Centre for Medium-Range Weather Forecasts ensemble prediction system. *Nat. Hazards Earth Syst. Sci.* **2020**, *20*, 2365–2378. [CrossRef]
41. Ziel, R.H.; Bieniek, P.A.; Bhatt, U.S.; Strader, H.; Rupp, T.S.; York, A. A Comparison of Fire Weather Indices with MODIS Fire Days for the Natural Regions of Alaska. *Forests* **2020**, *11*, 516. [CrossRef]
42. Hanes, C.C.; Wang, X.; Jain, P.; Parisien, M.; Little, J.M.; Flannigan, M.D. Fire-regime changes in Canada over the last half century. *Can. J. For. Res.* **2019**, *49*, 256–269. [CrossRef]
43. Di Giuseppe, F.; Pappenberger, F.; Wetterhall, F.; Krzeminski, B.; Camia, A.; Libertá, G.; San Miguel, J. The Potential Predictability of Fire Danger Provided by Numerical Weather Prediction. *J. Appl. Meteorol. Clim.* **2016**, *55*, 2469–2491. [CrossRef]
44. Wotton, B.M.; Nock, C.A.; Flannigan, M.D. Forest fire occurrence and climate change in Canada. *Int. J. Wildland Fire* **2010**, *19*, 253–271. [CrossRef]
45. Williams, A.P.; Abatzoglou, J.T.; Gershunov, A.; Guzman-morales, J.; Bishop, D.A.; Balch, J.K.; Lettenmaier, D.P. Observed Impacts of Anthropogenic Climate Change on Wildfire in California. *Earth's Future* **2019**, *7*, 892–910. [CrossRef]
46. Sedano, F.; Randerson, J.T. Multi-scale influence of vapor pressure deficit on fire ignition and spread in boreal forest ecosystems. *Biogeosciences* **2014**, *11*, 3739–3755. [CrossRef]
47. Gu, L.; Meyers, T.; Pallardy, S.G.; Hanson, P.J.; Yang, B.; Heuer, M.; Hosman, K.P.; Riggs, J.S.; Sluss, D.; Wullschleger, S.D. Direct and indirect effects of atmospheric conditions and soil moisture on surface energy partitioning revealed by a prolonged drought at a temperate forest site. *J. Geophys. Res. Atmos.* **2006**, *111*, D16102. [CrossRef]
48. Gamelin, B.L.; Feinstein, J.; Wang, J.; Bessac, J.; Yan, E.; Kotamarthi, V.R. Projected, U.S. drought extremes through the twenty-first century with vapor pressure deficit. *Sci. Rep.* **2022**, *12*, 8615. [CrossRef]
49. MTBS Data Access: Fire Level Geospatial Data MTBS Project (USDA Forest Service/U.S. Geological Survey). Available online: http://mtbs.gov/direct-download (accessed on 6 July 2023).
50. Town of Merrimack, New Hampshire Hazard Mitigation Plan Update 2021. p. 25. Available online: https://www.merrimacknh.gov/sites/g/files/vyhlif3456/f/uploads/merrimack_hazmit_update2021_final.pdf (accessed on 6 July 2023).
51. Copernicus Climate Change Service, Climate Data Store Fire Danger Indices Historical Data from the Copernicus Emergency Management Service. Available online: https://cds.climate.copernicus.eu/cdsapp#!/dataset/cems-fire-historical-v1?tab=form (accessed on 6 July 2023).
52. Wagner, V.C.E. *Development and Structure of the Canadian Forest Fire Weather Index System*; Forestry Technical Report; Canadian Forestry Service: Ottawa, ON, Canada, 1987; p. 35.
53. Wotton, B.M. Interpreting and using outputs from the Canadian Forest Fire Danger Rating System in research applications. *Environ. Ecol. Stat.* **2009**, *16*, 107–131. [CrossRef]
54. Touma, D.; National Center for Atmospheric Research Staff (Eds.) *The Climate Data Guide: Canadian Forest Fire Weather Index (FWI)*; 2023; Available online: https://climatedataguide.ucar.edu/climate-data/canadian-forest-fire-weather-index-fwi (accessed on 11 July 2023).
55. Hersbach, H.; Bell, B.; Berrisford, P.; Biavati, G.; Horányi, A.; Muñoz Sabater, J.; Nicolas, J.; Peubey, C.; Radu, R.; Rozum, I.; et al. ERA5 Hourly Data on Pressure Levels from 1940 to Present. Copernicus Climate Change Service (C3S) Climate Data Store (CDS). 2023. Available online: https://cds.climate.copernicus.eu/cdsapp#!/dataset/reanalysis-era5-pressure-levels?tab=overview (accessed on 20 June 2023).
56. Trenberth, K.E. Atmospheric Moisture Recycling: Role of Advection and Local Evaporation. *J. Clim.* **1999**, *12*, 1368–1381. [CrossRef]
57. Zhang, T.; Hoell, A.; Perlwitz, J.; Eischeid, J.; Murray, D.; Hoerling, M.; Hamill, T.M. Towards Probabilistic Multivariate ENSO Monitoring. *Geophys. Res. Lett.* **2019**, *46*, 10532–10540. [CrossRef]
58. Mantua, N.J.; Hare, S.R.; Zhang, Y.; Wallace, J.M.; Francis, R.C. A Pacific Interdecadal Climate Oscillation with Impacts on Salmon Production. *Bull. Amer. Meteor. Soc.* **1997**, *78*, 1069–1080. [CrossRef]
59. Bagley, R.B.; Clements, C.B. Extreme Fire Weather Associated with Nocturnal Drying in Elevated Coastal Terrain of California. *Mon. Weather. Rev.* **2021**, *149*, 2497–2511. [CrossRef]
60. Johnson, N.C.; Feldstein, S.B. The Continuum of North Pacific Sea Level Pressure Patterns: Intraseasonal, Interannual, and Interdecadal Variability. *J. Clim.* **2010**, *23*, 851–867. [CrossRef]
61. Abatzoglou, J.T.; Kolden, C.A.; Balch, J.K.; Bradley, B.A. Controls on interannual variability in lightning-caused fire activity in the western US. *Environ. Res. Lett.* **2016**, *11*, 045005. [CrossRef]
62. California Department of Water Resources. *California's Drought of 2007–2009*; 2010. Available online: https://water.ca.gov/SearchResults?sort=relevance&search=&tab=documents (accessed on 1 July 2024).

63. Varga, K.; Jones, C.; Trugman, A.; Carvalho, L.M.; McLoughlin, N.; Seto, D.; Thompson, C.; Daum, K. Megafires in a warming world: What wildfire risk factors led to California's largest recorded wildfire. *Fire* **2022**, *5*, 16. [CrossRef]
64. Goss, M.; Swain, D.L.; Abatzoglou, J.T.; Sarhadi, A.; Kolden, C.A.; Williams, A.P.; Diffenbaugh, N.S. Climate change is increasing the likelihood of extreme autumn wildfire conditions across California. *Environ. Res. Lett.* **2020**, *15*, 094016. [CrossRef]
65. Zhou, S.; L'Heureux, M.; Weaver, S.; Kumar, A. A composite study of the MJO influence on the surface air temperature and precipitation over the continental United States. *Clim. Dyn.* **2012**, *38*, 1459–1471. [CrossRef]
66. Diao, Y.; Li, T.; Hsu, P. Influence of the Boreal Summer Intraseasonal Oscillation on Extreme Temperature Events in the Northern Hemisphere. *J. Meteorol. Res.* **2018**, *32*, 534–547. [CrossRef]
67. Povak, N.A.; Kane, V.R.; Collins, B.M.; Lydersen, J.M.; Kane, J.T. Multi-scaled drivers of severity patterns vary across land ownerships for the 2013 Rim Fire, California. *Landsc. Ecol.* **2020**, *35*, 293–318. [CrossRef]
68. Hoell, A.; Hoerling, M.; Eischeid, J.; Wolter, K.; Dole, R.; Perlwitz, J.; Xu, T.; Cheng, L. Does El Niño intensity matter for California precipitation? *Geophys. Res. Lett.* **2016**, *43*, 819. [CrossRef]
69. Cole, J.E.; Overpeck, J.T.; Cook, E.R. Multiyear La Niña events and persistent drought in the contiguous United States. *Geophys. Res. Lett.* **2002**, *29*, 25-1–25-4. [CrossRef]
70. Wallace, J.M.; Hobbs, P.V. *Atmospheric Science: An Introductory Survey*; Elsevier: Amsterdam, The Netherlands, 2006; Volume 92.
71. Altman, N.; Krzywinski, M. Points of Significance: Association, correlation and causation. *Nat. Methods* **2015**, *12*, 899. [CrossRef] [PubMed]
72. Abatzoglou, J.T.; Williams, A.P. Impact of anthropogenic climate change on wildfire across western US forests. *Proc. Natl. Acad. Sci. USA* **2016**, *113*, 11770–11775. [CrossRef] [PubMed]
73. Westerling, A.L.; Hidalgo, H.G.; Cayan, D.R.; Swetnam, T.W. Warming and Earlier Spring Increase Western U.S. Forest Wildfire Activity. *Science* **2006**, *313*, 940–943. [CrossRef] [PubMed]
74. Barnes, E.A.; Samarasinghe, S.M.; Ebert-Uphoff, I.; Furtado, J.C. Tropospheric and stratospheric causal pathways between the MJO and NAO. *J. Geophys. Res. Atmos.* **2019**, *124*, 9356–9371. [CrossRef]
75. Zou, Y.; Rasch, P.J.; Wang, H.; Xie, Z.; Zhang, R. Increasing large wildfires over the western United States linked to diminishing sea ice in the Arctic. *Nat. Commun.* **2021**, *12*, 6048. [CrossRef]